Journal of
Materials Chemistry C

ROYAL SOCIETY
OF CHEMISTRY

PAPER

View Article Online
View Journal | View Issue

Check for updates

Cite this: *J. Mater. Chem. C*, 2023, **11**, 676

Organic microspheres and microcrystals made from pyridine-functionalized chromophores and a chiral phosphoric acid†

Li Meng,[ab] Zhong-Qiu Li,*[b] Kun Tang,[b] Jiang-Yang Shao, [b] Zili Chen *[a] and Yu-Wu Zhong *[bc]

Received 12th November 2022,
Accepted 6th December 2022

DOI: 10.1039/d2tc04818c

rsc.li/materials-c

Well-defined luminescent micro/nanostructures are important building blocks for miniaturized photonic devices. In this work, a simple method is employed to prepare organic microspheres and crystalline microrods with circularly polarized luminescence (CPL) properties. The *in situ* protonation and co-assembly of a series of pyridine-functionalized chromophores and a chiral binaphthol phosphoric acid give rise to blue-to-yellow emissive amorphous microspheres and green- and yellow-emissive crystalline microrods with good fluorescence quantum yields (9.6–64.6%). The luminescence dissymmetry factors (g_{lum}) of microrods ($\sim 10^{-3}$) are found to be one order of magnitude larger than those of microspheres. These microstructures and related materials are further characterized by fluorescence microscopy, scanning electron microscopy, single-crystal and powder X-ray diffraction, and Fourier transform-infrared spectroscopy analyses. The well-defined morphologies and promising luminescence properties of these microstructures make them potentially useful for chiral photonic applications.

Introduction

Materials with circularly polarized luminescence (CPL) properties have recently attracted considerable research attention due to their appealing application prospects in light-emitting devices, three-dimensional displays, catalysis, and optical information storage and encryption.[1–10] CPL can be generated from chiral single-component chromophores and assemblies or those consisting of multiple components. A great number of organic molecular materials have been reported to exhibit CPL activity by covalently linking chiral motifs with luminescent chromophores.[1–10] This method sometimes suffers from tedious synthesis. In comparison, self-assembly offers a simple and powerful strategy to obtain CPL *via* chirality transfer and amplification among constituent subunits.[11–20] Thanks to the noncovalent nature of chiral assembled systems, their CPL properties can be readily modulated by changing the assembly conditions or applying an external stimulus.[11–20]

Organic nanophotonics focus on the photonic studies of organic nanostructures or microstructures with well-defined morphologies, including the preparation of photofunctional structures with different dimensionalities and their applications in the fabrication of various miniaturized photonic devices such as lasers, waveguides, and logic gate circuits.[21–25] In this regard, organic nano/microstructures with CPL activity represent an advanced type of material allowing us to manipulate polarized light in photonic devices.[26–30] Among them, CPL-active structures with a one-dimensional (1D) or a two-dimensional (2D) shape can be relatively readily obtained.[26–30] In particular, this is true for those formed as a result of ordered or helical molecular packing, leading to efficient chirality transfer and/or chirality amplification. In comparison, zero-dimensional (0D) spherical micro/nanostructures with CPL activity are less known.[31,32] Micro/nanoparticles or spheres are typically amorphous and they are very likely CPL-inactive owing to the unordered molecular arrangement and irregular spatial organization of luminophores, though chiral molecular components are present in these structures.[33] Polymeric microspheres recently reported by Yamamoto and co-workers are one striking example, and they show a particularly high luminescence factor (g_{lum}) of 0.23 when dispersed in methanol.[34] The high g_{lum} value is related to the formation of a liquid crystalline mesosphere in these microspheres.

---

[a] *Department of Chemistry, Renmin University of China, 59# Zhongguancun Street, Haidian District, Beijing 100872, China. E-mail: zilichen@ruc.edu.cn*

[b] *Beijing National Laboratory for Molecular Sciences, CAS Key Laboratory of Photochemistry, CAS Research/Education Center for Excellence in Molecular Sciences, Institute of Chemistry, Chinese Academy of Sciences, 2 Bei Yi Jie, Zhong Guan Cun, Haidian District, Beijing 100190, China. E-mail: lizhongqiu@iccas.ac.cn, zhongyuwu@iccas.ac.cn*

[c] *School of Chemical Sciences, University of Chinese Academy of Sciences, No. 19(A) Yuquan Road, Shijingshan District, Beijing 100049, China*

† Electronic supplementary information (ESI) available: TDDTF results, single crystal X-ray diffraction data, and other supplementary data. CCDC 2210345 and 2210218. For ESI and crystallographic data in CIF or other electronic format see DOI: **https://doi.org/10.1039/d2tc04818c**

In chiral assemblies, noncovalent interactions, such as hydrogen bonding interactions, π–π stacking, and metal–metal interactions, play significant roles in determining their photophysical properties.[11–20] We recently employed the *in situ* reaction and crystallization of pyridine-functionalized chromophores with the chiral camphor sulfonic acid to prepare crystalline microplates with full-color CPL with g_{lum} in the order of 10^{-2} and high photoluminescence quantum yields (Φ_{PL}).[28] When treated with a strong protonic acid, these pyridine compounds are transformed into protonated pyridinium derivatives, to which the chiral sulfonic anions are bound by hydrogen bonding interactions in the solid state.[35–37] Pyridinium derivatives emit intense photoluminescence with a π/π* localized or intramolecular charge transfer (ICT) character, accompanied by distinct CPL due to the effective chirality transfer from chiral anions to pyridinium chromophores. Considering the widespread use of C_2-symmetric chiral binaphthyl phosphoric acids in organic catalysis[38,39] and the high utilities of binaphthyl frameworks in preparing CPL-active materials,[40–45] we are interested in examining the possibility of preparing CPL-active micro/nanostructures by the reaction of pyridine derivatives with the chiral binaphthyl phosphoric acid as a strong protonic acid. For this purpose, the reactions of (*R*/*S*)-1,1′-binaphthyl-2,2′-diyl hydrogenphosphate ((*R*/*S*)-BPA) with achiral pyridine-containing chromophores **1–5** have been attempted (Fig. 1; only (*R*)-BPA is displayed). By varying the preparation conditions, microspheres and crystalline microrods with multicolor CPLs have been obtained from this binary assembly, with g_{lum} in the order of 10^{-4} and 10^{-3}, respectively.

Results and discussion

Compounds **1–5** have a linear shape and consist of a phenylpyridine skeleton substituted with different aryl groups. They were prepared by the palladium-catalyzed Suzuki coupling or Heck reaction from 4-(*p*-bromophenyl)pyridine *via* reported procedures.[36] The attachments of various aryl groups are expected to expand the conjugation of these molecules, leading to the modulation of their assembly behaviours and emission properties.

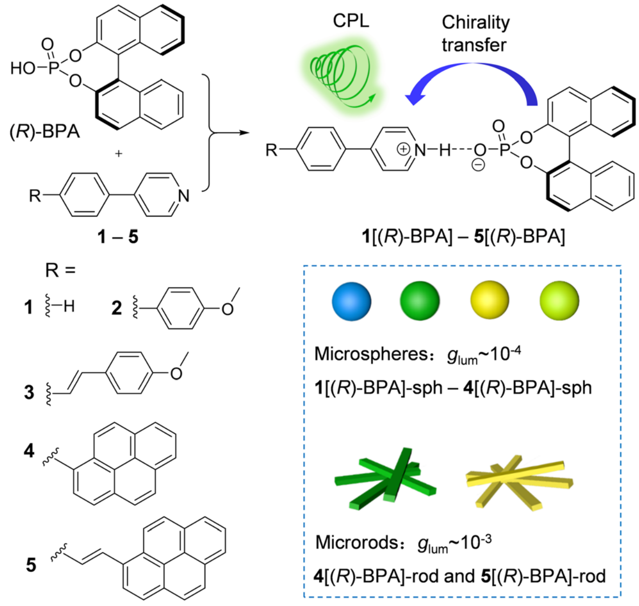

Fig. 1 Schematic diagram showing the reaction of (*R*)-BPA with **1–5** to give CPL-active microspheres and crystalline microrods.

Compounds **1–5** exhibit gradually red-shifted emissions in dichloromethane (CH_2Cl_2) solutions from **1** to **5**, with the emission maximum wavelength λ_{emi} varying from 335 to 461 nm (Table 1 and Fig. 2). Compounds **2–5** are highly emissive with fluorescence quantum yields (Φ_{FL}) of over 45%. However, the shortest compound **1** is only weakly emissive with a Φ_{FL} of 0.80%. The chiral acid (*R*)-BPA displays absorption between 250 and 340 nm with the absorption maximum wavelength λ_{abs} at 303 nm and an intense ultraviolet emission band with a λ_{emi} of 352 nm and a Φ_{FL} of 29.7% (Fig. S1, ESI†). The fluorescence emission lifetimes (τ) of these compounds are in the range of 0.32–2.34 ns.

When treated with (*R*)-BPA, distinct absorption spectral redshifts were observed for the solutions of **2–5** as a result of the protonation of the pyridine unit. However, such a spectral shift is less obvious for **1** due to the overlap between the absorption spectra of **1** and (*R*)-BPA. In the presence of (*R*)-BPA, the original emissions of **1–5** were diminished and a new emission band with a longer λ_{emi} appeared. The new emissions of the longer molecules **2–5** are attributed to the ICT process targeted at the pyridinium motif,[35–37] which is supported by the time-dependent density functional theory (TDDFT) calculations of the protonated cationic moieties (Fig. S2, ESI†). The emission of (*R*)-BPA is barely visible in the solutions of **2–5** in the presence of (*R*)-BPA, reflecting the efficient energy transfer between them. The emission spectral changes caused by the addition of acid are in agreement with the emission color changes of these compounds (Fig. 2k and 2l). The observed emission band of **1** in the presence of (*R*)-BPA is more likely associated with (*R*)-BPA based on the consistency of their emission wavelengths and the weak emission of **1**.

When treated with (*R*)-BPA or (*S*)-BPA, compounds **1–5** zshow mirror-image circular dichroism (CD) signals in CH_2Cl_2

Table 1 Photophysics data in CH_2Cl_2 solution[a]

Compound	λ_{abs}/nm	λ_{emi}/nm	Φ_{FL}[b]/%	τ/ns
(*R*)-BPA	303, 324	352	29.7	2.20
1	252	335	0.80	0.99
1 + (*R*)-BPA	289, 327	354	ND	ND
2	298	389	72.4	1.30
2 + (*R*)-BPA	303, 349	478	ND	ND
3	341	427	45.7	0.32
3 + (*R*)-BPA	280, 376	534	ND	ND
4	280, 346	427	50.7	2.34
4 + (*R*)-BPA	302, 360	564	ND	ND
5	312, 379	461	60.6	2.06
5 + (*R*)-BPA	302, 397	583	ND	ND

[a] Excitation wavelength: 260 nm for (*R*)-BPA and **1**; 280 nm for **2–4**; 300 nm for **5**. ND = not determined. The absolute Φ_{FL} values of the emissions of **1–5** with the addition of (*R*)-BPA have not been determined because the degrees of protonation and thus the emission intensities are dependent on the solution concentration. [b] Absolute fluorescence quantum yields (1×10^{-6} M).

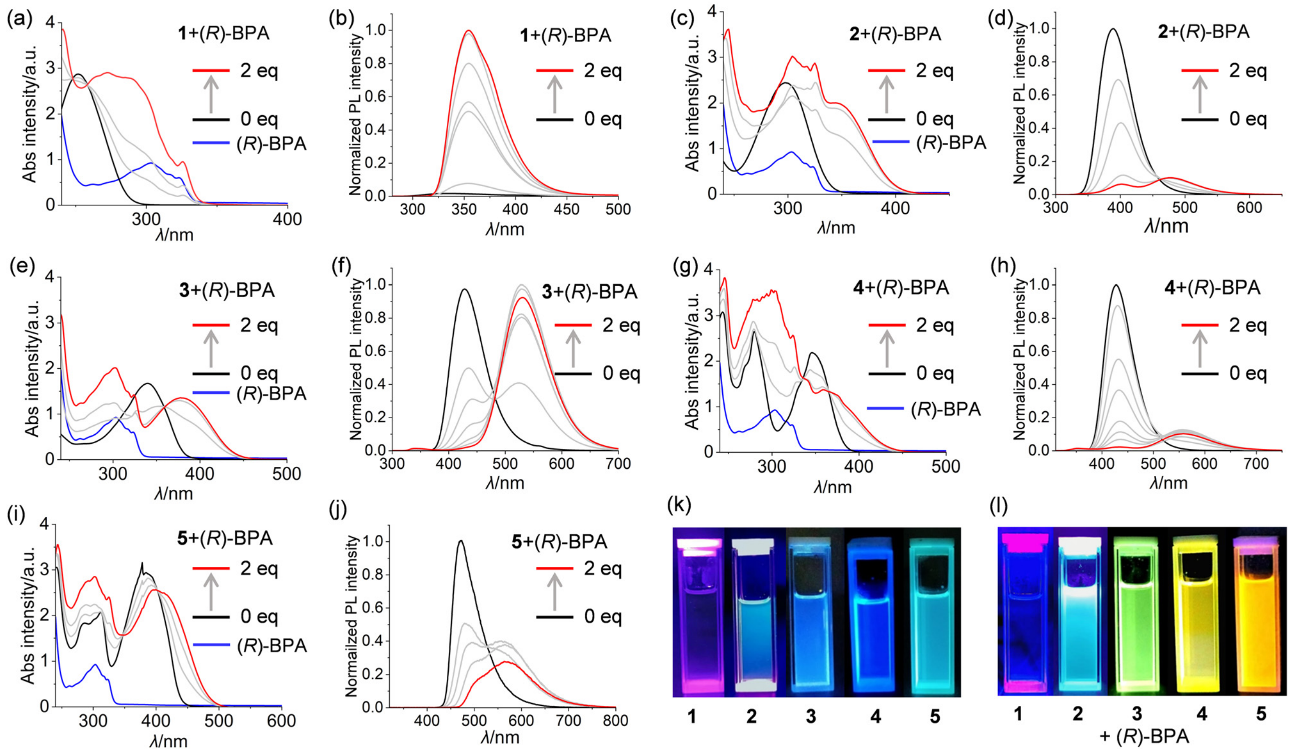

Fig. 2 (a, c, e, g, and i) Absorption and (b, d, f, h, and j) photoluminescence (PL) spectral changes of **1–5** upon the treatment of (*R*)-BPA (up to 2.0 equiv.) in CH_2Cl_2 (5×10^{-5} M). The absorption spectrum of (*R*)-BPA (blue curves) is included for the purpose of comparison. (k and l) Images of **1–5** in CH_2Cl_2 under UV illumination in the (k) absence and (l) presence of 2 equiv. of (*R*)-BPA (5×10^{-4} M). Excitation wavelength: 260 nm for **1**; 280 nm for **2–4**; and 300 nm for **5**.

(Fig. S3, ESI†). These signals are largely related to the chirality information of (*R*)-BPA or (*S*)-BPA in the wavelength range of 240–340 nm. The very weak CD signals in the longer wavelength region between 340 and 450 nm (except **1**) are associated with the ICT absorptions of the pyridinium compounds. However, the solutions of these protonated pyridinium molecules display no detectable CPL signals, suggesting that the excited-state chirality transfer is negligible in the solution state (Fig. S4, ESI†).

With the above solution-state spectral changes in mind, we embarked on the preparation of nanostructures or microstructures from the *in situ* reactions of **1–5** with (*R*/*S*)-BPA. To our delight, by natural solvent evaporation of a mixture of **1–4** with equal equiv. of (*R*/*S*)-BPA in mixed solvents of CH_2Cl_2/tetrahydrofuran (THF)/ethyl acetate (EA) (see details in the Experimental section), microspheres **1**[(*R*/*S*)-BPA]-sph–**4**[(*R*/*S*)-BPA]-sph with a diameter of 1.0–2.0 μm were obtained (Fig. 3 and Fig. S5 (ESI†); sph stands for microspheres). In this mixed solvent system, CH_2Cl_2 and THF behave as the good solvents; while EA is a poor solvent for the *in situ* formed pyridinium salt. When the solvents evaporate gradually, microspheres are generated on the quartz plate. The binary chemical compositions of these microspheres are supported by NMR and mass spectral analyses. The similar procedure for the reactions of **5** with (*R*/*S*)-BPA however only gave irregular solids. This difference may be caused by the relatively lower solubility of **5** and **5**[(*R*/*S*)-BPA] in these solvents. Microspheres **1**[(*R*/*S*)-BPA]-sph–**4**[(*R*/*S*)-BPA]-sph exhibit blue, green, yellow and green-yellow emissions, respectively. The λ_{emi} of **1**[(*R*/*S*)-BPA]-sph (470 nm) is distinctly red-shifted with respect to that of the mixed solution (354 nm) of **1** with (*R*)-BPA, probably caused by the molecular aggregation of BPA in the solid state. However, **2**[(*R*/*S*)-BPA]-sph–**4**[(*R*/*S*)-BPA]-sph (496, 552, and 540 nm, respectively) exhibit similar λ_{emi} with respect to corresponding solution mixtures (478, 534, and 564 nm, respectively), suggesting that similar protonated products are obtained in two states. Microspheres **1**[(*R*/*S*)-BPA]-sph have a τ of around 35 ns; however, **2**[(*R*/*S*)-BPA]-sph–**4**[(*R*/*S*)-BPA]-sph have a shorter τ of 3.93–4.54 ns (Table 2). This again reflects the different emission natures of these samples. All the samples exhibit moderate to good emission efficiencies, with Φ_{FL} values of 19.8%, 64.3%, 31.8% and 9.6% for **1**[(*R*/*S*)-BPA]-sph–**4**[(*R*/*S*)-BPA]-sph, respectively.

The above microsphere samples are essentially non-crystalline (see Discussion later). We are also interested in preparing well-defined organic crystals from the *in situ* reactions of **1–5** with (*R*/*S*)-BPA, in the hope of their potential applications in photonics.[21–25] In a previous study, we found that the reactions of these pyridine-functionalized chromophores in THF with perchloric acid ($HClO_4$) readily yielded plate-shaped microcrystals with appealing polarized emission properties.[36] However, when similar nanoprecipitation conditions were attempted with **1–5** and (*R*/*S*)-BPA, no crystals were formed due to the better solubilities of the resulting salts with respect to those with ClO_4^- counteranions. In this regard, other

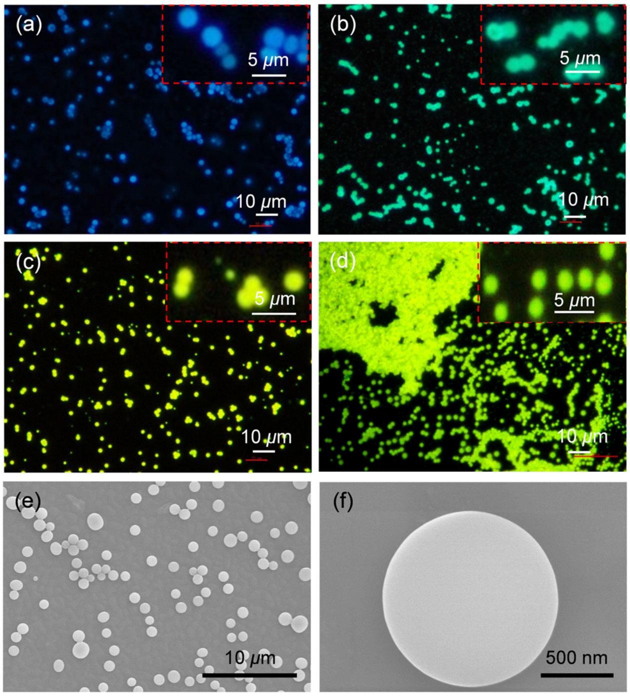

Fig. 3 (a–d) Fluorescence microscopy images of (a) **1**[(*R*)-BPA]-sph, (b) **2**[(*R*)-BPA]-sph, (c) **3**[(*R*)-BPA]-sph, and (d) **4**[(*R*)-BPA]-sph. The insets show the enlarged images of different spherical samples. (e and f) SEM images of microspheres **4**[(*R*)-BPA]-sph.

Table 2 CPL data of solid microspheres and microrods[a]

Compound	λ_{emi}/nm	$\Phi_{FL}{}^{b}$/%	τ/ns	$g_{lum}{}^{c}$ ($\times 10^{-4}$)
1[(*R*)-BPA]-sph	470	19.8	35.0	−2.99
1[(*S*)-BPA]-sph	470	20.7	35.1	+1.45
2[(*R*)-BPA]-sph	496	64.3	5.59	−2.18
2[(*S*)-BPA]-sph	496	64.4	5.58	+2.26
3[(*R*)-BPA]-sph	552	31.8	4.00	−4.62
3[(*S*)-BPA]-sph	552	32.4	3.93	+5.11
4[(*R*)-BPA]-sph	540	9.60	7.11	+2.92
4[(*S*)-BPA]-sph	540	10.5	7.54	−1.14
4[(*R*)-BPA]-rod	501	16.3	4.89	−18.4
4[(*S*)-BPA]-rod	501	17.2	4.64	+20.3
5[(*R*)-BPA]-rod	558	32.6	2.39	−17.7
5[(*S*)-BPA]-rod	558	31.7	2.31	+11.2

[a] Excitation wavelength: 345 nm for **1**[(*R*/*S*)-BPA]-sph; 400 nm for **2**[(*R*/*S*)-BPA]sph–**4**[(*R*/*S*)-BPA]-sph and 400 nm for **4**[(*R*/*S*)-BPA]-rod, 430 nm for **5**[(*R*/*S*)-BPA]-rod. [b] Absolute fluorescence quantum yields. [c] $g_{lum} = [2 \times (I_L - I_R)]/(I_L + I_R)$, where I_L and I_R stand for the emission intensities of left- and right-hand CPL, respectively. The values are determined by g_{lum} = [ellipticity/(32980/ln10)]/total fluorescence intensity at a specific emission wavelength.

reaction conditions were attempted. Gratifyingly, the natural evaporation of the solution of **4** with (*R*/*S*)-BPA in mixed CH_2Cl_2 and EA and the nanoprecipitation of **5** with (*R*/*S*)-BPA in mixed solvents of CH_2Cl_2 and THF gave rod-like microcrystals **4**[(*R*/*S*)-BPA]-rod and **5**[(*R*/*S*)-BPA]-rod, respectively (Fig. 4 and Fig. S6, ESI†). These microrods have lengths of 50–100 μm and diameters of 0.5–2 μm. They exhibit green and yellow emissions, with λ_{emi} values of 501 and 558 nm, respectively (Table 2).

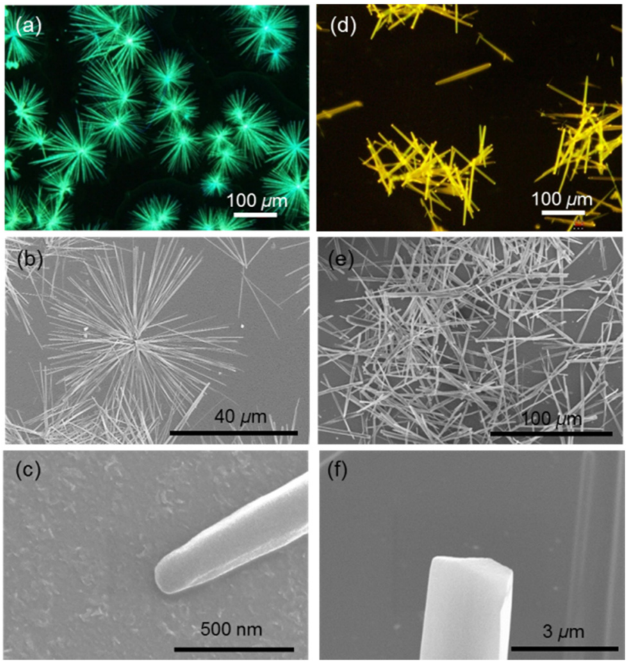

Fig. 4 (a and d) Fluorescence microscopy and (b, c, e, and f) SEM images of microrods (a–c) **4**[(*R*)-BPA]-rod and (d–f) **5**[(*R*)-BPA]-rod.

Notably, the emission of **4**[(*R*/*S*)-BPA]-rod (λ_{emi} = 501 nm) is somewhat blue-shifted with respect to those of **4**[(*R*/*S*)-BPA]-sph (λ_{emi} = 540 nm) and the solution mixture of **4** with (*R*/*S*)-BPA (λ_{emi} = 564 nm). In addition, the crystalline rod samples also exhibit higher Φ_{FL} values than spherical samples. The blue-shifted emissions of the crystalline samples are likely a result of the rigidification effect and their higher Φ_{FL} can be ascribed to the reduced non-radiative decays in crystals. λ_{emi} of **5**[(*R*/*S*)-BPA]-rod (558 nm) is also blue-shifted than that of the solution mixture of **5** with (*R*/*S*)-BPA (583 nm). Microcrystals **4**[(*R*)-BPA]-rod and **5**[(*R*)-BPA]-rod have τ of a few of ns and Φ_{FL} values of 16.3% and 32.6%, respectively (Table 2).

The chiral optical activities of microspheres **1**[(*R*/*S*)-BPA]-sph–**4**[(*R*/*S*)-BPA]-sph were examined by CD and CPL spectral analyses (Fig. 5). The pseudo-mirror-image CD spectra were recorded for these materials with (*R*)- and (*S*)-BPA. In addition, some weak CD signals beyond 350 nm are present for **2**[(*R*/*S*)-BPA]-sph–**4**[(*R*/*S*)-BPA]-sph. Because these signals are too weak, their absorption dissymmetry factors (g_{abs}) have not been determined. Depending on the molecular chirality of BPA, multicolor CPLs from 470 to 560 nm were recorded from these microspheres. Microspheres **1**[(*R*)-BPA]-sph–**3**[(*R*)-BPA]-sph show negative CPLs; while positive CPLs are observed for **1**[(*S*)-BPA]-sph–**3**[(*S*)-BPA]-sph. However, **4**[(*R*/*S*)-BPA]-sph microspheres show an opposite trend. The reason for this difference is not clear at this stage. The molecular aggregation in the solid state may result in different excited states. The luminescence factors g_{lum} of these CPLs are in the order of 10^{-4} at the maximum emission wavelength. Among them, **3**[(*R*/*S*)-BPA]-sph exhibit the highest g_{lum} with values of -4.62×10^{-4} and $+5.11 \times 10^{-4}$, respectively. Though the g_{lum} values of these

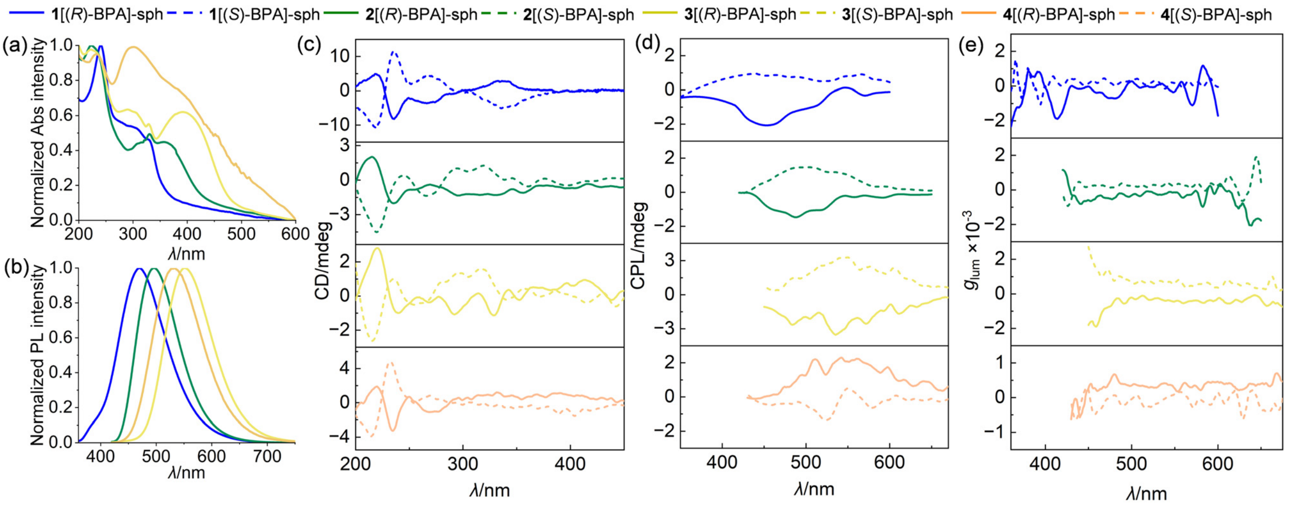

Fig. 5 (a) UV-vis absorption and (b) photoluminescence (PL) spectra of microspheres **1**[(*R*)-BPA]-sph–**4**[(*R*)-BPA]-sph. (c) CD, (d) CPL, and (e) g_{lum} spectra of microspheres **1**[(*R*/*S*)-BPA]-sph–**4**[(*R*/*S*)-BPA]-sph. Excitation wavelength: 345 nm for **1**[(*R*/*S*)-BPA]-sph and 400 nm for **2**[(*R*/*S*)-BPA]-sph–**4**[(*R*/*S*)-BPA]-sph, respectively.

microspheres are low, these results reflect that the excited-state chirality transfer from BPA is more effective in the solid state than that in the solution state. In the latter case, no CPLs could be observed at all (Fig. S4, ESI†).

In comparison to microspheres, microcrystals **4**[(*R*/*S*)-BPA]-rod and **5**[(*R*/*S*)-BPA]-rod are characterized with better CPL properties (Fig. 6). The distinct mirror image CD and CPL spectra have been obtained for crystals containing (*R*)- and (*S*)-BPA. The g_{lum} values are in the order of 10^{-3} at the maximum CPL wavelength. Microcrystals **4**[(*R*/*S*)-BPA]-rod show values of -1.85×10^{-3} and $+2.04 \times 10^{-3}$; while **5**[(*R*/*S*)-BPA]-rod possesses g_{lum} values of -1.77×10^{-3} and $+1.12 \times 10^{-3}$, respectively. These values are one order of magnitude larger than those of the above-discussed microspheres, suggesting the beneficial role of crystalline structures in promoting the chirality transfer. Considering that these samples are crystals, the CPL measurements may suffer from the influence of potential linearly polarized luminescence. In order to clarify this issue, the CPL spectra were subjected to repeated measurements by rotating the substrate to a certain degree (from 0° to 270°). Indeed, the CPL intensities and shapes only show a slight degree of variation during these measurements (Fig. S7, ESI†), supporting the reliabilities of the CPL and the g_{lum} data of these crystalline samples. In addition, in order to reduce the influence of the scattering effect during the measurement, the solid samples are placed in front of the detector as close as possible. The observations of the distinct mirror-image CD and CPL spectra of the rod samples (Fig. 6 and Fig. S7, ESI†) suggest that the influence of the scattering effect, in any, is insignificant.

In order to further probe the structures of the pyridine-functionalized compounds with BPA, the single crystals of

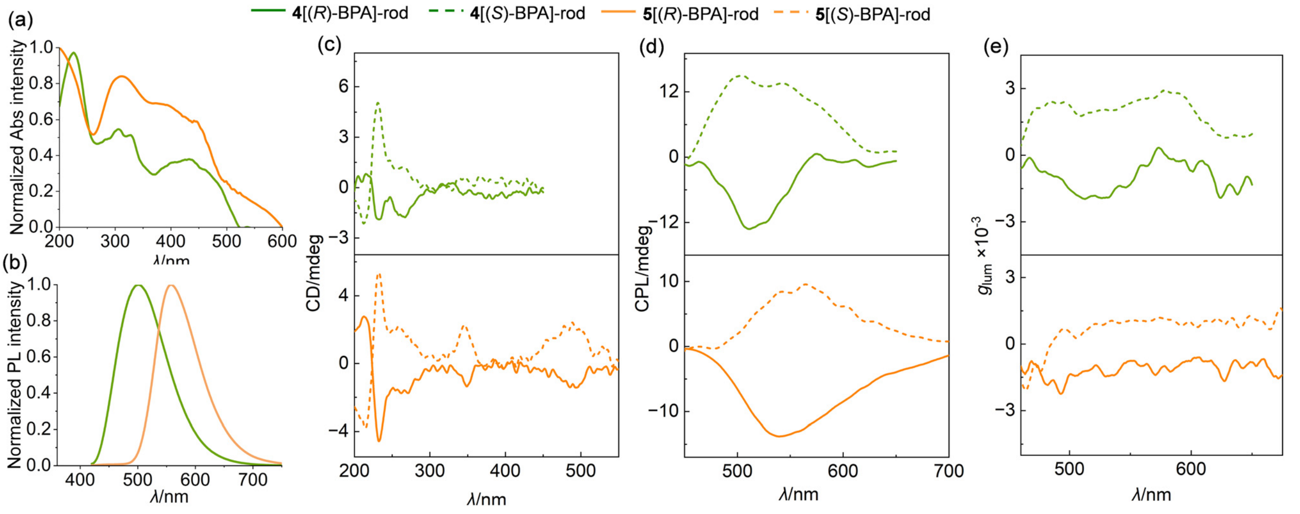

Fig. 6 (a) UV-vis absorption and (b) PL spectra of microrods **4**[(*R*)-BPA]-rod and **5**[(*R*)-BPA]-rod. (c) CD, (d) CPL, and (e) g_{lum} spectra of microrods **4**[(*R*/*S*)-BPA]-sph and **5**[(*R*/*S*)-BPA]-sph. Excited at 400 nm for **4**[(*R*/*S*)-BPA]-rod and 430 nm for **5**[(*R*/*S*)-BPA]-rod, respectively.

4[(*R*)-BPA] and **5**[(*R*)-BPA] have been obtained from the natural solvent evaporation of the solutions containing **4** with 1.0 equiv. of (*R*)-BPA in mixed CH_2Cl_2/THF/EA (2/1/8, v/v/v) and **5** with 1.0 equiv. of (*R*)-BPA in mixed CH_2Cl_2/THF (1/6, v/v), respectively. These crystals possess the chiral $C2$ and $P2_1$ space groups, respectively, and the corresponding crystallographic data are summarized in Table S1 (ESI†). In both cases, the pyridine groups are protonated by chiral BPA, and the pyridinium hydrogen atoms are linked to the oxygen atoms of BPA by a strong hydrogen bond with a NH···O distance of 1.75 Å (Fig. 7). Beside from these strong NH···O hydrogen bonds, some weak CH···O bonds are evident from the single-crystal X-ray analysis between some hydrogen atoms from aromatic rings and the phosphate oxygen atoms. These weak hydrogen bonds have longer H···O distances in the range of 2.40–2.63 Å. In addition, hydrogen bonding and some π–π interactions are observed in the molecular packing of these crystals, *e.g.* between the pyridinium groups and pyrene planes of **4**[(*R*)-BPA] (3.80 Å) and **5**[(*R*)-BPA] (3.53 Å) and among different pyridinium groups of **4**[(*R*)-BPA] (3.74 Å). When viewed from the *b*-axis of **4**[(*R*)-BPA], an alternating aromatic fragment and a phosphate lamellar structure are observed. In the case of **5**[(*R*)-BPA], head-to-tail dimeric stacking is observed among the long aromatic fragments and layered structures are evident when it is viewed from the *a*-axis. The hydrogen bonding interactions between the aromatic chromophores and the chiral BPA anions and the ordered molecular packings in the crystal structures are believed to play an important role in the chirality transfer.

The powder X-ray diffraction (PXRD) spectra of the microsphere samples **1**[(*R*)-BPA]-sph–**4**[(*R*)-BPA]-sph suggest that they are non-crystalline (Fig. 8; the broad peaks between 2θ of 15–30° are from the substrate background). In contrast, the high crystallinity of microcrystals is supported by the sharp diffraction peaks of **4**[(*R*)-BPA] at the (001) plane and **5**[(*R*)-BPA] at the (101) plane. This suggests that the ordered molecular arrangements of the crystalline samples are beneficial in enhancing the chirality transfer.

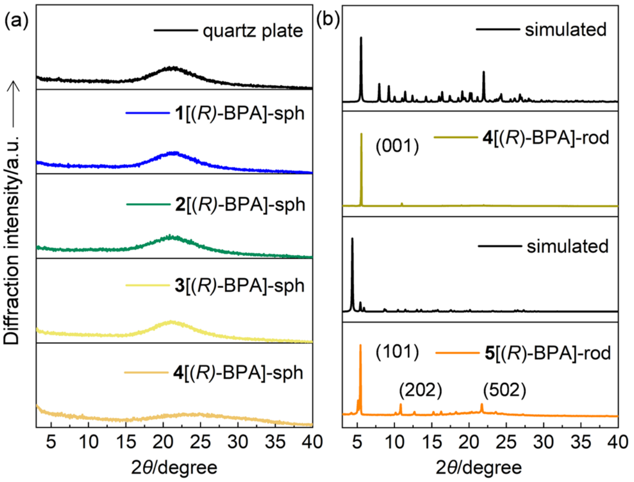

Fig. 8 PXRD patterns of (a) microspheres of **1**[(*R*)-BPA]-sph–**4**[(*R*)-BPA]-sph and (b) microrods of **4**[(*R*)-BPA]-rod and **5**[(*R*)-BPA]-rod. The data of the bare quartz substrate is included in panel (a) as a control sample. The simulated patterns of **4**[(*R*)-BPA] and **5**[(*R*)-BPA] are included in panel (b).

Fourier transform-infrared (FTIR) spectroscopy was further used to gain insight into the hydrogen bonding interactions in the microsphere and microcrystal samples. All these samples display an infrared (IR) peak at 3230–3250 cm^{-1}, which can be assigned to the pyridinium N–H stretching vibration (Fig. 9).[46] In contrast, compounds **1–5** are IR silent in this region (Fig. S8, ESI†). In addition, the P═O and P–O peaks of free BPA are located at 1228 cm^{-1} and 954 cm^{-1}, respectively.[47] In contrast, the P–O peaks of microspheres and microcrystals exhibit a slight shift to the higher wavenumber region (956–960 cm^{-1}) and their dominating P═O stretching vibrations appear

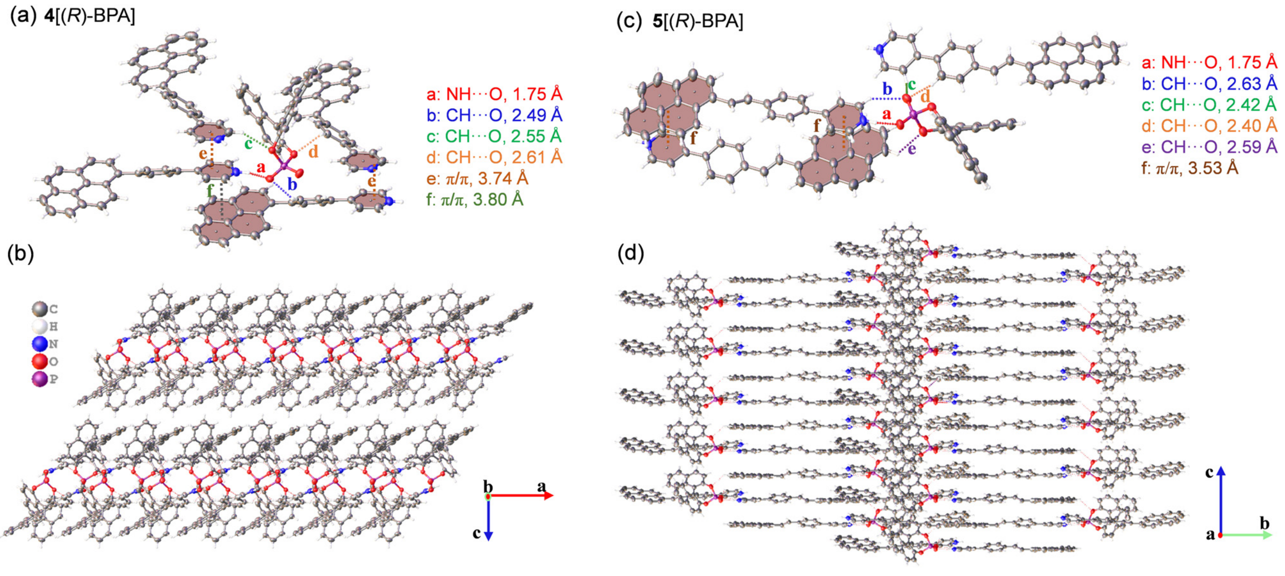

Fig. 7 Thermal ellipsoid plots at 30% probability of the single-crystal structures and crystal packing of (a and b) **4**[(*R*)-BPA] and (c and d) **5**[(*R*)-BPA].

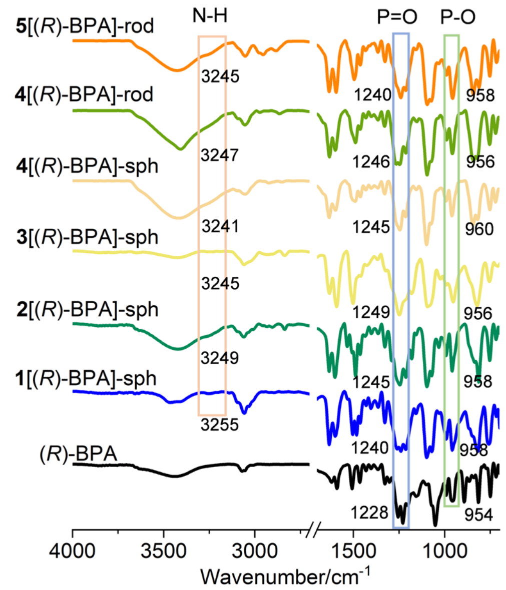

Fig. 9 FTIR spectra of (*R*)-BPA, microspheres of **1**[(*R*)-BPA]-sph–**4**[(*R*)-BPA]-sph and microrods of **4**[(*R*)-BPA]-rod and **5**[(*R*)-BPA]-rod as KBr pellets. The wavenumbers in cm^{-1} of N–H, P═O, and P–O vibrations are indicated in the figure.

between 1240 and 1249 cm^{-1}. These changes are in consistent with the presence of hydrogen bonding between pyridinium hydrogen and BPA oxygen atoms in both the microsphere and microcrystal samples.[48]

Conclusions

In summary, a convenient method for fabricating CPL-active multicolor microspheres and microcrystals is presented based on the reaction and co-assembly of pyridine-containing compounds with a chiral binaphthyl phosphoric acid. Four pairs of chiral microspheres with blue to yellow emissions have been obtained with g_{lum} in the order of 10^{-4}. Two pairs of microcrystals with green and yellow CPLs have been prepared with a higher g_{lum} in the order of 10^{-3}. The origins of CPLs are related to the chirality transfer from the chiral phosphoric framework to the conjugated pyridinium chromophores. The improved g_{lum} of microcrystals *versus* amorphous microspheres suggests that the ordered molecular packing in the crystalline samples plays a role in boosting the CPL performance. The relatively low g_{lum} values may be partially caused by the long distance between the chiral binaphthyl framework and the pyridinium moieties. In the future, we intend to use chiral binaphthyl phosphoric acids with steric bulky substituents to prepare microstructures,[38,39] which may be helpful in improving the CPL properties. In addition, these CPL-active microspheres and microcrystals with well-defined shapes are believed to have potential for chiroptical applications as optical resonators and building blocks for photonic devices.[21–25]

Experimental

Instrumental information for physical measurements

The UV-vis absorption spectra were recorded at rt using the TU-1810DSPC spectrometer from Beijing Purkinje General Instrument Co., Ltd. The photoluminescence spectra were recorded at rt using an F-380 spectrofluorimeter from Tianjin Gangdong Sci. & Tech. Development Co., Ltd. The absolute fluorescence quantum yields were determined using a Hamamatsu Absolute PL Quantum Yield Spectrometer C11347 with the aid of an integrating sphere. The Hamamatsu C11367-11 instrument with single photon counting was employed to obtain the excited-state lifetimes. The morphologies of microstructures were investigated by SEM using a Hitachi SU8010 instrument at 10 kV. A Rigaku Saturn 724 diffractometer was used to perform the single-crystal X-ray analysis at 173 K in a rotating anode (Cu Kα; λ = 1.54184 Å). The structures were solved with SHELXS-97 and refined on Olex2. The crystallographic data are summarized in Table S1 (ESI†). The powder X-ray diffraction (PXRD) was carried out using a Rigaku D/max-2500 instrument (Cu Kα; λ = 1.54 Å). The fluorescence microscopy characterization was run using an Olympus IX83 Inverted fluorescence microscope by UV irradiation at 325–375 nm. A JASCO J-1700 spectrometer was used to obtain the CD spectra. The JASCO CPL-300 spectrometer was used to record the CPL spectra. The Bruker VERTEX 70v spectrometer was used to record the FTIR spectra.

Methods for TDDFT calculations

The electronic structures of [**1**-H]$^+$–[**5**-H]$^+$ were first optimized using the Gaussian 09 program package by density functional theory (DFT) calculations with B3LYP/6-31G** and the consideration of the solvent (CH_2Cl_2) effect. TDDFT calculations were carried out on the optimized structures with a long-range correlated CAM-B3LYP functional.[49]

Synthesis and characterization

General information. Compounds **1–3** and **5** are known and prepared according to literature studies.[36] Compound **4** was prepared using a similar procedure as described below. Because of the overlap of signals, the numbers of the observed ^{13}C NMR peaks are smaller than expected.

Synthesis of 4-((pyren-1-yl)phen-4-yl)pyridine (4). To a solution of 4-(bromophen-4-yl)pyridine (500 mg, 2.14 mmol) and 1-pyrenylboronic acid (1.053 g, 4.28 mmol) in 20 mL of THF, tetrakis(triphenylphosphine)palladium (70 mg, 0.060 mmol) was added. A solution of K_2CO_3 (1.48 g, 10.7 mmol) in 10 mL of water was then added. The reaction mixture was bubbled with nitrogen for 10 min, followed by stirring at 95 °C for 12 h. After cooling to room temperature, THF was evaporated. The crude product was extracted with copious CH_2Cl_2. The organic phase was then washed with brine and dried over $MgSO_4$. The product was purified by column chromatography on silica gel using petroleum ether/ethyl acetate 5/1 as the eluent and was obtained as a faint yellow solid (483.2 mg) in 63.5% yield. ^{1}H NMR (400 MHz, $CDCl_3$): δ 8.77–8.69 (d, J = 5.3 Hz, 2H), 8.28–8.17 (m, 4H), 8.13 (s, 2H), 8.10–7.98 (m, 3H), 7.82 (dd, J = 12.7 8.7 Hz, 4H), 7.65 (d, J = 5.6 Hz, 2H).

^{13}C NMR (75 MHz, CDCl$_3$): δ 150.42, 147.94, 142.17, 136.96, 136.70, 131.49, 131.37, 130.95, 130.87, 128.49, 127.76, 127.67, 127.48, 127.41, 127.01, 126.14, 125.32, 125.00, 124.89, 124.73, 121.60. HRMS (MALDI) calcd for [M]$^+$ C$_{27}$H$_{17}$N: 355.1356. Found: 355.1356.

Synthesis of microspheres 1[(*R*/*S*)-BPA]-sph. To a solution of **1** (500 μL, 6.44 mM, 0.0032 mmol) in CH$_2$Cl$_2$, (*R*)-BPA (190 μL, 16.8 mM, 0.0032 mmol) was added in THF. The mixed solution was injected into 1.0 mL of ethyl acetate. The solution was transferred to a quartz plate by direct dropping. The solvent volatilized naturally to give **1**[(*R*)-BPA]-sph as white microspheres on the plate, which were directly used for various measurements. ^{1}H NMR (400 MHz, CD$_2$Cl$_2$): δ 8.47 (d, *J* = 5.9 Hz, 2H), 7.92 (dd, *J* = 14.2, 8.5 Hz, 4H), 7.70 (d, *J* = 5.7 Hz, 2H), 7.61 (d, 2H), 7.58–7.48 (m, 5H), 7.43 (t, *J* = 7.2 Hz, 2H), 7.35 (d, *J* = 8.5 Hz, 2H), 7.26 (t, *J* = 8.0 Hz, 2H). ^{13}C NMR (100 MHz, CDCl$_3$): δ 156.02, 148.67, 148.58, 141.83, 134.50, 132.42, 131.47, 131.28, 130.59, 129.53, 128.31, 127.53, 127.02, 126.13, 124.93, 123.23, 122.02, 122.00, 121.72, 121.70. ESI-HRMS (P) calcd for C$_{11}$H$_{10}$N [M − BPA + H]$^+$: 156.0808; found: 156.0808. Microspheres **1**[(*S*)-BPA]-sph were prepared using the same method as **1** and (*S*)-BPA.

Synthesis of microspheres 2[(*R*/*S*)-BPA]-sph. To a solution of **2** (500 μL, 7.65 mM, 0.0038 mmol) in CH$_2$Cl$_2$, (*R*)-BPA (110 μL, 34.5 mM, 0.0038 mmol) in THF was added. The mixture was then injected into 3.0 mL of ethyl acetate. The solvent volatilized naturally to afford **2**[(*R*)-BPA]-sph as green microspheres on the plate. ^{1}H NMR (400 MHz, CD$_2$Cl$_2$): δ 8.46 (d, *J* = 5.9 Hz, 2H), 7.92 (dd, *J* = 16.0, 8.0 Hz, 4H), 7.78–7.65 (m, 6H), 7.61 (d, *J* = 8.8 Hz, 2H), 7.57 (d, *J* = 8.8 Hz, 2H), 7.43 (t, *J* = 7.2 Hz, 2H), 7.35 (d, *J* = 8.5 Hz, 2H), 7.25 (t, *J* = 7.0 Hz, 2H), 7.02 (d, *J* = 8.8 Hz, 2H), 3.86 (s, 3H). ^{13}C NMR (100 MHz, CDCl$_3$): δ 160.00, 153.58, 149.26, 149.17, 144.04, 143.55, 133.43, 132.58, 131.94, 131.19, 130.40, 128.26, 128.22, 127.81, 127.59, 127.06, 126.05, 124.78, 122.43, 122.29, 122.27, 121.99, 121.97, 114.54, 55.42. ESI-HRMS (P) calcd for C$_{18}$H$_{16}$NO [M − BPA + H]$^+$: 262.1226; found: 262.1225. Microspheres **2**[(*S*)-BPA]-sph were prepared using the same method as **2** and (*S*)-BPA.

Synthesis of microspheres 3[(*R*/*S*)-BPA]-sph. To a solution of **3** (500 μL, 6.96 mM, 0.0035 mmol) in CH$_2$Cl$_2$ was added (*R*)-BPA (102 μL, 34.5 mM, 0.0036 mmol) in THF. The mixture was then injected into 4.0 mL of ethyl acetate. The solvent volatilized naturally to give **3**[(*R*)-BPA]-sph as yellow microspheres on the plate. ^{1}H NMR (400 MHz, CD$_2$Cl$_2$): δ 8.43 (d, *J* = 5.9 Hz, 2H), 7.92 (dd, *J* = 14.1, 8.5 Hz, 4H), 7.71 (d, *J* = 5.7 Hz, 2H), 7.67–7.47 (m, 8H), 7.43 (t, *J* = 7.5 Hz, 2H), 7.36 (d, *J* = 8.6 Hz, 2H), 7.29 – 7.20 (m, 3H), 7.03 (d, *J* = 16.3 Hz, 1H), 6.94 (d, *J* = 8.3 Hz, 2H), 3.84 (s, 3H). ^{13}C NMR (100 MHz, CDCl$_3$): δ 160.02, 155.00, 149.03, 148.93, 142.23, 141.27, 132.76, 132.54, 131.25, 131.20, 130.48, 129.40, 128.29, 128.19, 127.84, 127.25, 127.07, 126.09, 124.85, 124.79, 122.55, 122.19, 122.17, 121.88, 121.86, 114.35, 55.39. ESI-HRMS (P) calcd for C$_{20}$H$_{18}$NO [M − BPA + H]$^+$: 288.1383; found: 288.1381. Microspheres **3**[(*S*)-BPA]-sph were prepared using the same method from **3** and (*S*)-BPA.

Synthesis of microspheres 4[(*R*/*S*)-BPA]-sph. A solution of **4** (500 μL, 5.63 mM, 0.0028 mmol) in CH$_2$Cl$_2$ was added (*R*)-BPA (250 μL, 11.48 mM, 0.0028 mmol) in THF. The mixture was then injected into 2.0 mL of ethyl acetate. The solvent volatilized naturally to afford **4**[(*R*)-BPA]-sph as green-yellow microspheres on the plate. ^{1}H NMR (400 MHz, DMSO-d$_6$): δ 8.81 (d, *J* = 6.6 Hz, 2H), 8.41 (d, *J* = 7.9 Hz, 1H), 8.35 (d, *J* = 7.6 Hz, 1H), 8.31 (d, *J* = 6.7 Hz, 1H), 8.26 (s, 2H), 8.24 – 8.18 (m, 3H), 8.18–8.06 (m, 7H), 8.03 (d, *J* = 8.1 Hz, 2H), 7.85 (d, *J* = 8.3 Hz, 2H), 7.52–7.44 (m, 4H), 7.35–7.30 (m, 2H), 7.22 (d, *J* = 8.5 Hz, 2H). ^{13}C NMR (100 MHz, DMSO-*d*$_6$): δ 170.78, 152.96, 149.41, 149.32, 144.86, 143.47, 136.29, 134.47, 132.26, 131.82, 131.43, 131.10, 131.00, 130.82, 128.95, 128.52, 128.37, 128.23, 128.09, 128.03, 127.83, 127.00, 126.90, 126.51, 126.07, 125.66, 125.50, 125.39, 124.74, 124.63, 124.46, 123.35, 122.46, 122.43, 121.92, 121.90. ESI-HRMS (P) calcd for C$_{27}$H$_{18}$N [M − BPA + H]$^+$: 356.1434; found: 356.1438. Microspheres **4**[(*S*)-BPA]-sph were prepared using the same method from **4** and (*S*)-BPA.

Synthesis of microcrystals 4[(*R*/*S*)-BPA]-rod. A solution of **4** (5.0 mg, 0.0141 mmol) and (*R*)-BPA (5.0 mg, 0.0143 mmol) in 2 mL of CH$_2$Cl$_2$ was injected into 0.5 mL of ethyl acetate. The solvent volatilized naturally to provide **4**[(*R*)-BPA]-rod as green microcrystals on the plate. The characterization data are the same as those of the above-prepared microspheres **4**[(*R*)-BPA]-sph. Microcrystals **4**[(*S*)-BPA]-rod were prepared using the same method from **4** and (*S*)-BPA.

Synthesis of microcrystals 5[(*R*/*S*)-BPA]-rod. To a solution of **5** (3.0 mL, 1.75 mM, 0.0052 mmol) in CH$_2$Cl$_2$ was added (*R*)-BPA (100 μL, 34.5 mM, 0.0052 mmol) in THF under ultrasonication. The ultrasonication was continued for 2 min. After aging for 30 min at rt, **5**[(*R*)-BPA]-rod appeared as yellow microcrystals on the bottom of the vial. ^{1}H NMR (400 MHz, DMSO-d$_6$): δ 8.90–8.69 (m, 3H), 8.65–8.53 (m, 2H), 8.38–8.26 (m, 4H), 8.20 (s, 2H), 8.17–8.02 (m, 11H), 7.67 (d, *J* = 16.1 Hz, 1H), 7.50–7.45 (m, 4H), 7.33 (t, *J* = 7.7 Hz, 2H), 7.22 (d, *J* = 8.6 Hz, 2H). ^{13}C NMR (100 MHz, DMSO-d$_6$): δ 149.59, 149.50, 146.28, 140.30, 134.87, 132.30, 131.65, 131.52, 131.12, 131.08, 131.06, 130.95, 130.67, 128.93, 128.57, 128.40, 128.30, 128.18, 127.94, 127.90, 127.27, 126.89, 126.81, 126.51, 125.98, 125.82, 125.71, 125.29, 124.80, 124.55, 124.04, 123.84, 122.65, 122.54, 122.52, 121.93, 121.91. ESI-HRMS (P) calcd for C$_{29}$H$_{20}$N [M − BPA + H]$^+$: 382.1589; found: 382.1590. Microcrystals **5**[(*S*)-BPA]-rod were prepared using the same method from **5** and (*S*)-BPA.

Preparation of single crystals. Single crystals of **4**[(*R*)-BPA] were obtained by natural solvent evaporation of the solution of **4** (0.51 mM) containing 1.0 equiv. of (*R*)-BPA in mixed CH$_2$Cl$_2$/THF/EA (2 mL/1 mL/8 mL). Single crystals of **5**[(*R*)-BPA] were obtained by natural solvent evaporation of the solution of **5** (0.82 mM) containing 1.0 equiv. of (*R*)-BPA in mixed THF/CH$_2$Cl$_2$ (1 mL/6 mL).

Conflicts of interest

There are no conflicts to declare.

Acknowledgements

Financial supports from the National Natural Science Foundation of China (grants 21925112, 22090021, 21872154, 21871294, and 21975264), the Youth Innovation Promotion Association CAS, and the Beijing Natural Science Foundation (grant 2191003) are acknowledged.

References

1 Z.-L. Gong, X. Zhu, Z. Zhou, S.-W. Zhang, D. Yang, B. Zhao, Y.-P. Zhang, J. Deng, Y. Cheng, Y.-X. Zheng, S.-Q. Zang, H. Kuang, P. Duan, M. Yuan, C.-F. Chen, Y. S. Zhao, Y.-W. Zhong, B. Z. Tang and M. Liu, *Sci. China: Chem.*, 2021, **64**, 2060–2104.

2 L. Arrico, L. Di Bari and F. Zinna, *Chem.*, 2021, **27**, 2920–2934.

3 D.-W. Zhang, M. Li and C.-F. Chen, *Chem. Soc. Rev.*, 2020, **49**, 1331–1343.

4 F. Pop, N. Zigon and N. Avarvari, *Chem. Rev.*, 2019, **119**, 8435–8478.

5 C. Zhang, S. Li, X.-Y. Dong and S.-Q. Zang, *Aggregate*, 2021, **2**, e48.

6 Y. Zhang, Y. Shu, H. Bing, Y. Zhou, X. Zhang, X. Gao and Z. Tang, *Matter*, 2022, **5**, 837–875.

7 C. Li, X. Jin, J. Han, T. Zhao and P. Duan, *J. Phys. Chem. Lett.*, 2021, **12**, 8566–8574.

8 X. Shang, L. Wan, L. Wang, F. Gao and H. Li, *J. Mater. Chem. C*, 2022, **10**, 2400–2410.

9 J. L. Greenfield, J. Wade, J. R. Brandt, X. Shi, T. J. Penfold and M. J. Fuchter, *Chem. Sci.*, 2021, **12**, 8589–8602.

10 Y.-P. Zhang, S.-Q. Song, M.-X. Mao, C.-H. Li, Y.-X. Zheng and J.-L. Zuo, *Sci. China: Chem.*, 2022, **65**, 1347–1355.

11 Y. Sang, J. Han, T. Zhao, P. Duan and M. Liu, *Adv. Mater.*, 2020, **32**, e1900110.

12 J. Kumar, T. Nakashima and T. Kawai, *J. Phys. Chem. Lett.*, 2015, **6**, 3445–3452.

13 Y. Deng, M. Wang, Y. Zhuang, S. Liu, W. Huang and Q. Zhao, *Light: Sci. Appl.*, 2021, **10**, 76.

14 F. Song, Z. Zhao, Z. Liu, J. W. Y. Lam and B. Z. Tang, *J. Mater. Chem. C*, 2020, **8**, 3284–3301.

15 Z.-L. Gong, Z.-Q. Li and Y.-W. Zhong, *Aggregate*, 2022, **3**, e177.

16 J. Zhao and P. Xing, *ChemPhotoChem*, 2022, **6**, e202100124.

17 X. Dou, N. Mehwish, C. Zhao, J. Liu, C. Xing and C. Feng, *Acc. Chem. Res.*, 2020, **53**, 852–862.

18 T. Zhao, J. Han, P. Duan and M. Liu, *Acc. Chem. Res.*, 2020, **53**, 1279–1292.

19 Z.-L. Gong and Y.-W. Zhong, *Sci. China: Chem.*, 2021, **64**, 788–799.

20 C. Xu, C. Yin, W. Wu and X. Ma, *Sci. China: Chem.*, 2022, **65**, 75–81.

21 Y. Yan and Y. S. Zhao, *Chem. Soc. Rev.*, 2014, **43**, 4325–4340.

22 Y.-L. Shi, M.-P. Zhuo, X.-D. Wang and L.-S. Liao, *ACS Appl. Nano Mater.*, 2020, **3**, 1080–1097.

23 Y. Huang, Z. Wang, Z. Chen and Q. Zhang, *Angew. Chem., Int. Ed.*, 2019, **58**, 9696–9711.

24 S. Li, Y. Hao, S. Guo, C. Ding, Y. Ma, R. Liu and D. Yan, *Sci. China: Chem.*, 2021, **65**, 408–417.

25 R. Li, Z.-L. Gong, Q. Zhu, M.-J. Sun, Y. Che, J. Yao and Y.-W. Zhong, *Sci. China: Chem.*, 2021, **65**, 328–338.

26 X. Ye, B. Li, Z. Wang, J. Li, J. Zhang and X. Wan, *Nat. Commun.*, 2021, **12**, 6841.

27 Z. Huang, T. Jiang, J. Wang, X. Ma and H. Tian, *Angew. Chem., Int. Ed.*, 2021, **60**, 2855–2860.

28 Z.-Q. Li, Z.-L. Gong, J.-Y. Shao, J. Yao and Y.-W. Zhong, *Angew. Chem., Int. Ed.*, 2021, **60**, 14595–14600.

29 N. Mitetelo, D. Venkatakrishnarao, J. Ravi, M. Popov, E. Mamonov, T. V. Murzina and R. Chandrasekar, *Adv. Optical Mater.*, 2019, **7**, 1801775.

30 W. Shang, X. Zhu, T. Liang, C. Du, L. Hu, T. Li and M. Liu, *Angew. Chem., Int. Ed.*, 2020, **59**, 12811–12816.

31 M. Li, C. Zhang, L. Fang, L. Shi, Z. Tang, H. Y. Lu and C. F. Chen, *ACS Appl. Mater. Interfaces*, 2018, **10**, 8225–8230.

32 J. Kumar, T. Nakashima, H. Tsumatori and T. Kawai, *J. Phys. Chem. Lett.*, 2014, **5**, 316–321.

33 Y. Wang, D. Niu, G. Ouyang and M. Liu, *Nat. Commun.*, 2022, **13**, 1710.

34 O. Oki, C. Kulkarni, H. Yamagishi, S. C. J. Meskers, Z. H. Lin, J. S. Huang, E. W. Meijer and Y. Yamamoto, *J. Am. Chem. Soc.*, 2021, **143**, 8772–8779.

35 Z.-Q. Li, J.-H. Tang, Y.-Q. He, Z.-L. Gong, J.-Y. Shao and Y.-W. Zhong, *Cryst. Growth Des.*, 2021, **21**, 1854–1860.

36 Z.-Q. Li, D.-X. Ma, F.-F. Xu, T.-X. Dan, Z.-L. Gong, J.-Y. Shao, Y. S. Zhao, J. Yao and Y.-W. Zhong, *Angew. Chem., Int. Ed.*, 2022, **61**, e202205033.

37 J.-Y. Zhao, F.-F. Xu, Z.-Q. Li, Z.-L. Gong, Y.-W. Zhong and J. Yao, *Materials*, 2022, **15**, 7247.

38 R. Maji, S. C. Mallojjala and S. E. Wheeler, *Chem. Soc. Rev.*, 2018, **47**, 1142–1158.

39 Z.-L. Xia, Q.-F. Xu-Xu, C. Zheng and S.-L. You, *Chem. Soc. Rev.*, 2020, **49**, 286–300.

40 R. Liu, B. Ding, D. Liu and X. Ma, *Chem. Eng. J.*, 2021, **421**, 129732.

41 K. Takaishi, S. Murakami, F. Yoshinami and T. Ema, *Angew. Chem., Int. Ed.*, 2022, **61**, e202204609.

42 K. Fu, X. Jin, M. Zhou, K. Ma, P. Duan and Z. Q. Yu, *Nanoscale*, 2020, **12**, 19760–19767.

43 K. Xiao, Y. Xue, B. Yang and L. Zhao, *CCS Chem.*, 2020, **2**, 555–565.

44 S.-P. Wan, H.-Y. Lu, M. Li and C.-F. Chen, *J. Photochem. Photobio. C*, 2022, **50**, 100500.

45 Z. Geng, Y. Zhang, Y. Zhang, Y. Li, Y. Quan and Y. Cheng, *J. Mater. Chem. C*, 2021, **9**, 12141–12147.

46 L. Li, Y. Hua, X. N. Li, Y. Guo and H. Zhang, *Dalton Trans.*, 2019, **48**, 10683–10688.

47 C. Koy, M. Michalik, G. Oehme, C. Fischer, A. Tillack, H. Baudisch and R. Kempe, *Phosphorus, Sulfur Silicon Relat. Elem.*, 2006, **152**, 203–228.

48 T. Dorn, A.-C. Chamayou and C. Janiak, *New J. Chem.*, 2006, **30**, 156–167.

49 T. Yanai, D. P. Tew and N. C. Handy, *Chem. Phys. Lett.*, 2004, **393**, 51–57.